Characteristics of Rainstorms over a Temperate Region Derived from Multiple Time Series of Weather Radar Images

[1] Mr. Ashis Kumar Das [*], [2] Mrs. Sipra Mohapatra
[1]Asst. Professor, Dept. OF Civil Engineering, NIT BBSR,*
Asst. Professor DEPT. of Civil Engineering, NIT, Nayagarh
[1]sipramohapatra@thenalanda.com , dasashish@gmail.com*

Abstract

Rainstorms can be geographically and temporally characterised with the help of weather radars. Correctly describing rainfall over time and space advances hydrological modelling and design, ultimately leading to better water management. Frontal rain systems over Belgium (Western Europe) are examined to offer a stochastic rainfall model with an accurate parameterization. The movement of rainstorms is examined in this work along with various structures within them and their respective spatial placements. Distribution functions are also created to statistically characterise various rainstorm characteristicsTo ascertain the direction and speed of the translation of storms, a correlation technique is used. Radar scans isolate well-developed rainstorms, which can then be examined for size and shape. Three approaches to describing the rainstorms' dimensions are suggested and contrasted. Probability distributions for rainfall dimensions, perimeter, area, velocity, and direction are provided through statistical analysis. In addition, the spatial distribution of clusters during a downpour is investigated. It is demonstrated that a straightforward Poisson process works effectively to represent this spatial distribution. In 1D and 2D, two approaches to calculating the single parameter in a Poisson process are suggested and contrasted..

Keywords: Weather radar; Rainstorm structure; Storm movement; Cluster Poisson process; Statistical distribution

1. Introduction

A crucial component of the hydrological cycle is rainfall. its significance in the generation of floods, erosion, the creation of biomass, biochemistry, and the distribution of energy

There is no denying the effects climate change will have on water quality (indirectly by its effect on soil moisture). In numerous study fields, including agriculture, hydrology, meteorology, climatology, and environmental engineering, the significance of rainfall variability is becoming increasingly clear. Classical measure-ments of rainfall by rain gauges give good estimates of temporal variation of rainfall, but estimates of spatially averaged rainfall based on rain gauge data donot fully take into account the spatial variability of

rainfall, unless high densities of rain gauges are installed (Shih, 1982; Peters-Lidard and Wood, 1994). Ever since rainstorms were first observed as noise with early military radars, hydrologists have held out hope that radars could reliably estimate rainfall. Today's weather radar images provide researchers with large amounts of spatial and temporal information on rainfall to overcome the current obstacle of poorly defined rainfall characteristics. During last decades, several studies have shown that hydrological models give better results when the spatial variability of the rainfall input is taken into account (De Troch et al., 1990; Krajewski et al., 1991; Obled et al., 1994; Shah et al., 1996; Willems and Berlamont, 1999; Chaubey et al., 1999; Arnaud et al., 1999). When performing a hydrological simulation using uniform rainfall over the catchment, the peak discharges might be overestimated, if occasionally the rain gauge measures a high intensity in a storm, since in reality the highest rainfall intensities will not occur over the whole catchment at the same time. As a consequence rainfall generators, which preserve the spatial organization of rainfall patterns, are necessary for simulating long time series of spatial rainfall that can be used in hydrological engineering studies. Improved hydrological forecasting and water resources management are expected, once accurate descriptions of rainfall patterns are implemented.

In general the pattern of rainfall is depending on the type of rainfall, typically classified (Bergeron, 1960; Bruce and Clark, 1996) as convective rainfall, orographic or relief rainfall, convergent rainfall and frontal or cyclonic rainfall. Austin (1960) and Austin and Houze (1972) described a consistent structure in rainfall patterns, based on the dimensions and lifetime of subsynoptic-scale rain areas (see Fig. 1). Synoptic areas are larger than 10^4 km^2 and have a lifetime of one to several days. The largest subsynoptic areas within a synoptic area are called large mesoscale areas (LMSA) which range between 10^3 and 10^4 km^2 and last for several hours. They are also named 'bands' by Amorocho and Wu (1977), because of their shape in the events studied. Next, small mesoscale areas (SMSA) are identified which cover 100–400 km^2 and have a life span of approximately an hour. Convective cells, which are generally clustered, are the smallest structural units. They range from 10 to 30 km^2 in extent and last only a few minutes to about

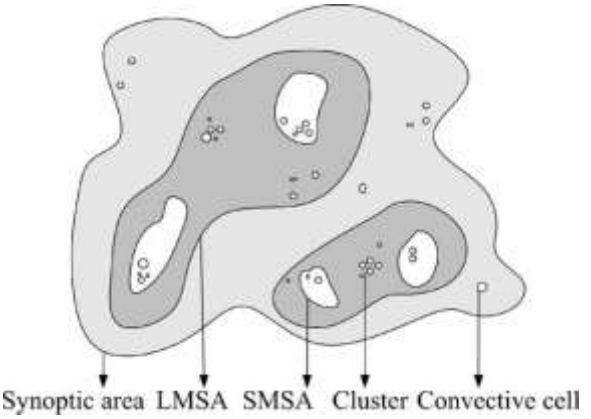

Fig. 1. Hierarchical structure of rainfall patterns.

half an hour. Although the short lifetime and the relative small extent of SMSAs and convective cells seem to make these subsynoptic areas relatively unsignificant within the complete synoptic event, their existance should be considered, as the smaller the scale, the higher the rainfall intensity will be. Heylen and Maenhout (1994) indicated that the scale of magnitude or the extent L (in meters), and the lifetime l (in seconds) of atmospheric events are related to each other by the approximate expression $\log(L)/\log(l) \approx 1$. Several authors report on the quantification of geometric characteristics of structural units within rain patterns (Mason, 1970; Hobbs and Locatelli, 1978; Gupta and Waymire, 1979; Niemczynowicz and Jönsson., 1981; Krajewski et al., 1993; Jinno et al., 1993; Berndtsson et al., 1994; Mellor and O'Connell, 1996; Bacchi et al., 1996; Kawamura et al., 1997; Willems, 2001).

The consistent occurrence and structure of subsynoptic-scale rain areas with similar characteristics and behavior is widely accepted and used in several attempts to model spatial rainfall (Waymire and Gupta, 1981a; Amorocho and Wu, 1977; Le Cam, 1961; Bras and Rodr´ıguez-Iturbe, 1976; Eagleson, 1984; Rodr´ıguez-Iturbe, 1986; Waymire, 1984; Váldes et al., 1985; Kavvas and Puri, 1983; Krajewski et al., 1993; Mellor, 1996; Rodr´ıguez-Iturbe and Eagleson, 1987; Willems, 2001). Evidently, the accuracy of such models is completely dependent on the correct parameterization and quantification of rainfall structures.

The objective of this study is to get an accurate description of some rainfall characteristics at the mesoscale. The results are of direct use in spatial rainfall generators, especially for the one being developed for the Flanders region (Belgium) (Willems, 2001). The velocity of rainfall events, the direction in which they move and the dimensions of rainstorms are studied thoroughly. The velocity of rain events and the direction of movement are best calculated using the correlation technique (Zawadski, 1973). This technique was applied with success by several authors during the last decades (Bonser and Wong, 1987; Mellor and O'Connell, 1996; Tsanis et al., 2002; Upton, 2002).

Besides the characterization of individual rainstorms, the positions of structures relative to each other within a rainstorm are of major importance and are therefore also studied in this paper. A wide range of point process rainfall generators are developed during the last decades (Waymire and Gupta, 1981a, b). A description of the temporal rainfall process is often based on Poisson processes: examples of well known models are the Poisson White Noise model (Gelfand and Vilenkin, 1964), the Independent Poisson Marks model (Eagleson, 1972), the Poisson Rectangular Pulses model (Rodr´ıguez-Iturbe, and Eagleson, 1987) and cluster Poisson models such as the Neyman-Scott White Noise model (Obeysekera et al., 1987), the Neyman-Scott Rectangular Pulses model (Rodr´ıguez-Iturbe, 1986) and the Bartlett-Lewis Rectangular Pulses model (Cox and Isham, 1980). An example of the extent of the clustered point process models in space are the models described by Cowpertwait (1995) and Cowpertwait et al. (2002). Based on the Taylor hypothesis (Taylor, 1938; Zawadski, 1973; Gupta and Waymire, 1987; Kumar and Foufoula-Georgiou, 1993), stating that rainfall fields are statistically homogeneous in time, spatial characteristics can be deduced from temporal characteristics in rainfall. This explains why Poisson fields are also often assumed to represent the spatial distribution of cells and clusters in many existing time-space rainfall generators.

The spatial rainfall model of Willems (2001), which also makes use of these Poisson fields, has been developed for application in urban hydrological problems. Therefore they made use of data obtained from a dense tipping bucket raingauge network, in order to parameterize the spatial properties of rainstorms up to the spatial level of small mesoscale areas. As their model can also describe the large mesoscale areas, additional analysis based on weather radar imagery, as described in this paper, is needed for their model. A complete explanation on the construction of the model can be found in Willems (2001).

This paper is structured as follows: after a description of the data (Section 2), the movement of rainy areas on radar images is studied (Section 3), a definition for fully developed rainstorms is formulated (Section 4) and methods to calculate geometric characteristics of rainstorms are proposed (Section 5). Finally, the spatial distribution of clusters (Section 6) is evaluated. Statistical descriptors and distributions (Section 7) of rainfall characteristics, determined in this study, can be used as an input for a stochastic spatial rainfall generator, such as the one currently being developed for the Flanders region (Belgium) (Willems, 2001).

2. Data description

Pseudo Constant Altitude Plan Position (pseudo-CAPPI) radar images, provided by the Royal Meteorological Institute of the Netherlands (KNMI), are used for the analyses presented in this paper. These images are covering the Netherlands, the western part of Germany and the northern part of Belgium. The images are produced by a combination of raw data from two C-band Doppler weather radars in De Bilt (52.1027$_8$ NW, 5.178$_8$ EL) and in Den Helder (52.9538$_8$ NW, 4.7909$_8$ EL) in the Netherlands. Both radars operate at four elevations (0.3, 1.1, 2.0 and 3.0$_8$) with an identical frequency of 5.6 GHz. The antenna heights of the weather radars in De Bilt and Den Helder are, respectively, 44 and 51 m a.s.l.. The reflectivity images of both radars are combined into a common grid in order to minimize noise and clutter echoes. The resulting product is a square image parallel to the meridian of Greenwich, with a 200X 200 pixel grid with pixel size 2.4X2.4 km^2. To transform the reflectivity values Z (mm^6 m^{K3}) into rainfall rates R (mm h^{K1}) the Marshall–Palmer formula, $ZZ200R^{1.6}$ (Marshall and Palmer, 1948), is used. The resulting rainfall rates are then grouped into

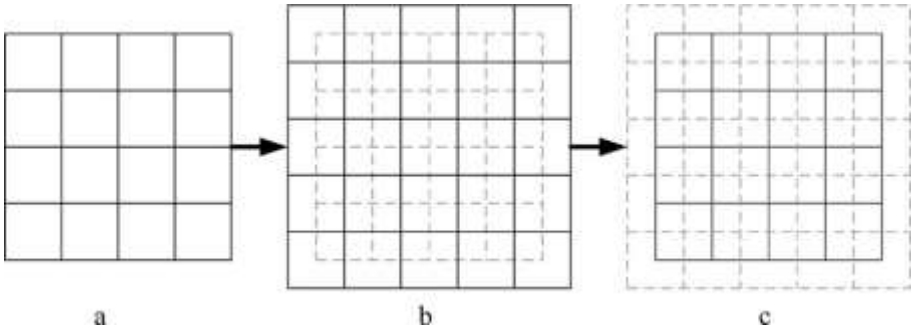

Fig. 2. Preprocessing of the radar data. (a) Class values are replaced by the average intensity value of the class. (b) Increase of image dimensions and resampling by averaging over a 2X2 window. (c) Splines interpolation of resampled intensities to the original grid.

eight classes, to facilitate visual interpretation. This product is delivered by the KNMI.

Preprocessing of these images includes reconverting class values to intensity values, resampling and splines interpolation as illustrated in Fig. 2. By this preprocessing algorithm the absolute values of the intensities may not always be retrieved perfectly (a separate study showed an R^2 of more than 0.85 between original and retrieved images), but it does not change the results in this paper, as only the position of clusters is of importance and not their absolute intensities.

Every 15 min an instantaneous radar observation is available, so for one complete day there are 96 images in one series. Due to problems in data acquisition or processing, some radar images are missing, resulting in gaps in the time series. The gaps most frequently consist in consecutive missing images.

Twenty series of radar images with at least 45 images per series are selected over the period 1998–2000 and a total of 1632 images are analyzed. To include possible seasonal variation, rainfall events are chosen throughout the year. Only rain events (excluding frozen precipitation) are selected and days with a relatively high amount of total daily rainfall are chosen. The dates, the number of images and the total amount of rain for every selected day are given in Table 1. Based on information provided by the Royal Meteorological Institute of Belgium (KMI, 1998–2000), we can conclude that all studied rainfall events are part of frontal weather systems. Most of these fronts are related to low pressure systems over the Atlantic Ocean causing maritime air mass movements over the studied region.

3. Movement of rain events

$R(x,y,t)$ is the rainfall intensity R in function of space (x,y) in a Cartesian coordinate system and time (t). The x-axis is chosen along the East–West direction of the radar images, whereas the y-axis corresponds with the North–South direction. Methods to monitor rain events $R(x, y)$ through time are mainly developed for forecast purposes (Chen and Kavvas, 1992; Brémaud and Pointin, 1993; Bellon and Zawadski, 1994; Burlando et al., 1996). A treatment of translation and rotation separately is rather exceptional and most reported methods are restricted to a monitoring of the translation. Methodologies to track the movement of rainstorms can be divided into 'pattern matching' and 'correlation' (Bonser and Wong, 1987). Once rainstorms are isolated, the simplest way to find the vector of translation is to

Table 1
Overview of selected days, number of images N and total amount of rainfall

Date (d/m/y)	N	Total rainfall (mm/day)	Date (d/m/y)	N	Total rainfall (mm/day)
06/03/98	96	23.2	31/10/98	96	32.6
07/04/98	96	30.6	26/11/98	45	10.5
27/04/98	59	6.9	15/12/98	60	3.1
23/08/98	96	35.0	30/05/99	96	33.0
25/08/98	76	1.6	04/06/99	96	30.0
01/08/98	53	0.7	04/07/99	96	57.4
02/09/98	94	7.3	26/12/99	96	33.5
13/09/98	96	93.6	16/05/00	74	6.9
24/10/98	96	19.3	03/06/00	82	18.2
27/10/98	80	2.5	02/07/00	49	13.6

determine the movement of the centers of the storms. In this study the translation of the mass centers of individual rainstorms as well as the mass centers of the whole rainy areas in radar images are followed.

In order to find the direction and the velocity of rainstorm translation for all pairs of radar images, a procedure is developed to find the movement vector for which the largest overlap between consecutive images is obtained and thus for which the correlation is maximal. A practical expression for the computation of the correlation coefficient r for the rainstorms on radar images is given by:

$$r(k_x, k_y) = \frac{\sum_{i=i_{min}}^{i_{max}} \sum_{j=j_{min}}^{j_{max}} [R(x_i, y_j, t) - m_t][R(x_i + k_x, y_j + k_y, t + t_d) - m_{t+t_d}]}{\left\{\sum_{i=i_{min}}^{i_{max}} \sum_{j=j_{min}}^{j_{max}} [R(x_i, y_j, t) - m_t]^2 \sum_{i=i_{min}}^{i_{max}} \sum_{j=j_{min}}^{j_{max}} [R(x_i + k_x, y_j + k_y, t + t_d) - m_{t+t_d}]^2\right\}^{1/2}} \quad (1)$$

with

$$m_t = \frac{\sum_{i=i_{min}}^{i_{max}} \sum_{j=j_{min}}^{j_{max}} R(x_i, y_j, t)}{N(k_x, k_y)} \quad (2)$$

$$m_{t+t_d} = \frac{\sum_{i=i_{min}}^{i_{max}} \sum_{j=j_{min}}^{j_{max}} R(x_i + k_x, y_j + k_y, t + t_d)}{N(k_x, k_y)} \quad (3)$$

with i and j, respectively, the row and column numbers of the pixels in the radar images. N is the number of pixels in the overlapping area of two consecutive images. The lower left corner of this overlapping area is indicated with coordinates (i_{min}, j_{min}), whereas the upper right corner is given by the coordinate couple (i_{max}, j_{max}). k_x and k_y, the spatial horizontal and vertical lag, are allowed to have all possible real values. However, because a minimum overlap of images is needed to calculate a representative value for the correlation, the spatial lags are limited to a maximum of 30 pixels. As will be shown, the velocity to cross 30 pixels in 15 min (i.e. 288 km h^{K1}) will never be reached in the studied time series.

As an accurate determination of the velocity and the direction of the movement is desirable, minor increments in movement lags are needed. In order to allow small movement lags, Mellor and O'Connell (1996) for example performed a mesh refinement followed by a parabolic interpolation of the surface. Then they investigated the movement over integer numbers of smaller pixels. An alternative approach is suggested here. The technique consists in translating the first image over all possible movement vectors (for all possible lengths and angles). Each time, the first image is resampled to the grid of the second image by calculating new pixels as weighted averages, where the weights correspond to the portions of the translated pixels covering a new pixel. There is always a smoothing or filtering of the first image, except for movements that are an integer multiple of the pixel size in as well the *x*- as the *y*-direction. The increments can be chosen as small as desired, evidently at the cost of computation time.

The translation (k_x, k_y) corresponding to the highest correlation (Eq. 1) between consecutive images, yields direct information on the angle of the direction q (rad) in which the rainfall event is moving relative to the *x*-axis and on the velocity u_{xy}

$$q = \arctan\frac{k_y}{k_x} \quad (4)$$

$$u_{xy} = \frac{\sqrt{k_x^2 + k_y^2}}{t_d} \quad (5)$$

with t_d the 15 min time lag between consecutive radar images.

4. Determination of rainfall structures in radar images

Methods to isolate rainfall structures in radar images are developed in order to quantify their geometric characteristics. Rainy areas in an image are defined as groups of pixels receiving rainfall, while a rain event covers all rainy areas in an image. A rainstorm is defined as the largest connected rainy area in a radar image. For the analysis only well developed rainstorms are selected, while rainstorms in development or decay are excluded. Furthermore, only rainstorms which are completely (or at least for the largest part) situated within the image boundaries

are useful. Therefore, a new concept, namely the APratio (km) is introduced:

$$\text{APratio} = \frac{\sum_{i=0}^{N} \text{Area } A_i}{\sum_{i=0}^{N} \text{Perimeter } P_i} \quad (6)$$

with N the number of individual rainy areas within the radar image. When a rainstorm is growing or dissipating, typically several small rainy areas can be detected in the image. This results in a relatively low APratio, because of the high total perimeter. Comparison of the time series of the APratio with the actual radar images also reveals that the APratio increases and decreases, when a rain event is entering or leaving the image box, because of a varying fractional coverage.

The temporal evolution of the APratio is plotted for every series of radar images and windows with information of interest, i.e. high APratio and well developed rainstorms, are selected (e.g. for October 24, 1998, Fig. 3). The APratio shows a similar temporal pattern for rainfall areas above different levels of intensity. The thresholds for the APratio, above which the rainy area can be considered to be fully developed, are different for each time series and are based on visual interpretation of the plots. However, as a general guideline, thresholds are chosen halfway the increasing and decreasing limbs of the curves for the APratios calculated for all rainfall areas (intensityO0 mm h^{K1}) (see Fig. 3 in which the dashed horizontal lines represent these thresholds). Finally, in each selected image the largest connected area with rainfall is selected as the rainstorm (Fig. 4). From the 1632 available radar images, only 934 were considered for further treatment, as they contained rainstorms that are (i) well developed and (ii) completely or at least for the largest part situated within a radar image.

Clusters and SMSAs are defined as groups of cells and are recognizable in radar images by the locally increased intensity of rainfall. Because the resolution of the images is too coarse to distinguish between clusters and SMSAs, both are named clusters in the remainder of this paper. The difficulty in automated determination of clusters is that the increased rainfall intensity is dependent on the position of the cluster in the rainstorm. The overall rainfall intensity changes within a rainstorm and therefore a fixed threshold cannot be used. A fixed threshold could exclude clusters located in a low intensity area, while it does not allow to distinguish between cluster centers within a high intensity area of the rainstorm. To deal with this problem, a level slicing method with variable thresholds is proposed. Therefore, only values within each image, larger than a threshold are maintained. In the resulting image, all groups of connected pixels are identified and an isolated group of minimal 8 pixels (or 46 km^2) is identified as a cluster of cells, only if its

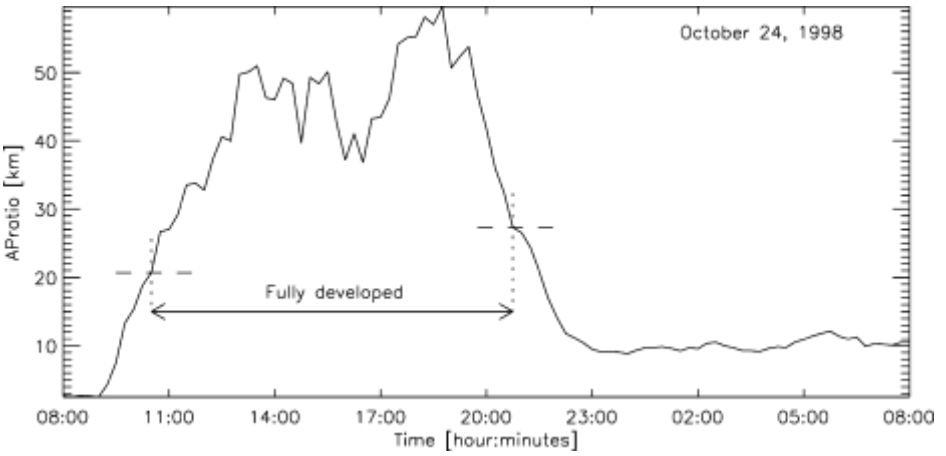

Fig. 3. APratio for the rainfall event at October 24, 1998 for rainy areas with intensities above the level of 0 mm h^{K1}: the APratio is calculated for all rainy areas. Only images with rainy areas characterized by Apratios above the dashed horizontal lines are assumed to show well developed rainstorms.

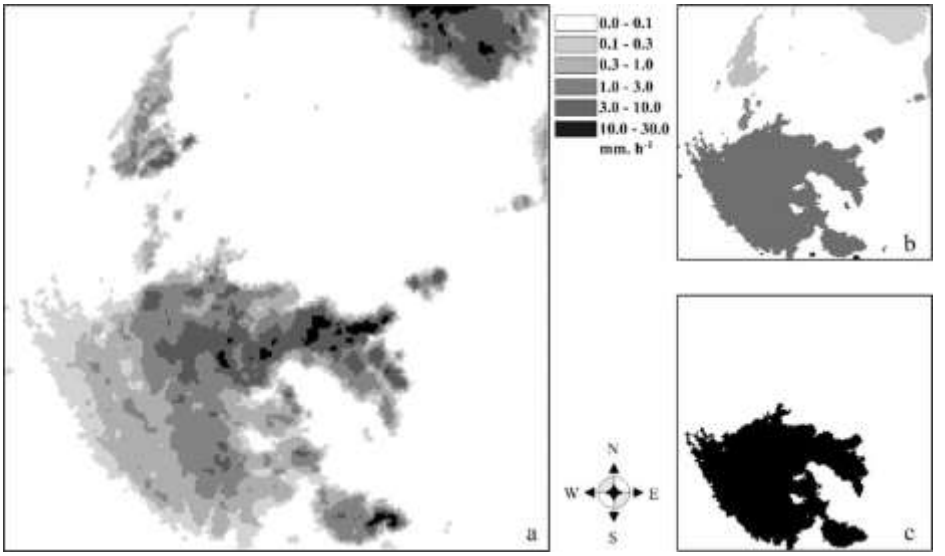

Fig. 4. Processing steps to select the rainstorm. (a) Original radar image for July 5, 1999 at 4:15 a.m. local time. (b) The different groups of connected pixels with rain are identified, and (c) only the largest group is selected as the rainstorm.

size becomes smaller than 8 pixels when, in a next step, the image is level sliced with a slightly higher threshold. The level slicing with increasing thresholds is repeated until no connected groups larger than 8 pixels are longer present in the resulting image. In that way, all clusters of cells in the image could be identified. The value of 46 km^2 was chosen in correspondence to literature (Mason, 1970; Niemczynowicz and Jönsson, 1981; Berndtsson and Niemczynowicz, 1986; Mellor and O'Connell, 1996).

5. Geometric description of rainfall structures

Different methods to characterize rainfall structures on radar images have been reported, mainly for statistical analyses and in procedures for forecasting (Collier, 1989). Well-known are descriptions using contour vectors, Fourier series expansions as applied by Blackmer and Duda (1972) or descriptions by a certain surface shape, e.g. a not-normalized bivariate distribution (Wiggert et al., 1976), which allows a description of the internal distribution of rainfall intensities. In this study a geometric approach is developed, which allows a straightforward implementation of the derived parameters into spatial rainfall models. A structure is described by its dimensions in two perpendicular directions. In a spatial rainfall generator, a rainfall structure is often represented by an ellipse, for which the axes can be defined by the determined dimensions. However, difficulties arise through the irregular shape of rainstorms. Three methods are proposed, as illustrated in Fig. 5.

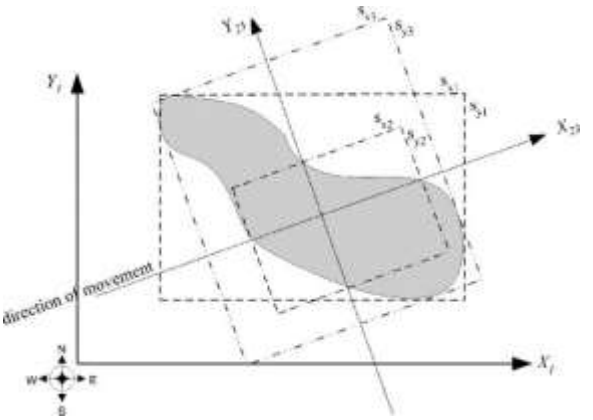

Fig. 5. Schematic overview of the three methods applied to determine the dimensions of a rainstorm. The rectangular in dash–dash line defines the dimensions of a rainstorm for method 1, in dash–dash–dot line for method 2 and in dash–dot–dot line for method 3.

Method 1

The maximum dimensions of the rainstorm are measured in the East–West and North–South directions of the image, defining the X_1–Y_1 coordinate system (Fig. 5). The smallest rectangle surrounding the rainstorm, with sides parallel to the X_1 and Y_1 axes, is used to determine the extent of the rainstorm. The lengths of the rectangle sides, s_{x1} and s_{y1}, are a first estimation of the rainstorm extent.

Method 2

A new coordinate system is defined with axes parallel (X_{23}) and perpendicular (Y_{23}) to the direction of movement of the rainstorm. The instantaneous direction of the movement at time t is defined as the average of the direction of the movement during the intervals $[t\text{Kt}_d,t]$ and $[t,t\text{Ct}_d]$. The origin of the axis is chosen in the center point (mp_x, mp_y) of the storm, where

$$mp_x = \frac{1}{N}\sum_i\sum_j x_i \text{ and } mp_y = \frac{1}{N}\sum_i\sum_j y_i \qquad (7)$$

for i and j over all pixels with intensities larger than 0 mm h^{K1} and N the number of pixels in the rainstorm. x_i and y_j are the x- and y-coordinate of a pixel within the rainstorm, measured along the X_1 and Y_1 axes. The intersections of the rainstorm with the X_{23} and Y_{23} axes form the boundaries for a rectangle (Fig. 5). The lengths of its sides give an estimation for the spatial extent of the rainstorm. The dimensions of the rainstorm parallel with and perpendicular to the direction of the movement are given by s_{x2} and s_{y2}, respectively.

Method 3

The same coordinate system as in method 2 is used, but now the dimensions of the rainstorm are defined by creating the smallest rectangle possible surrounding the rainstorm with its sides parallel to the X_{23} and Y_{23} axes (Fig. 5). The lengths of the rectangle sides (s_{x3} and s_{y3}) are used as measure for the dimensions of the rainstorm.

6. Spatial distribution of clusters

A simple Poisson process is often used to represent the distribution of clusters in time and space. The Poisson distribution is discrete and assumes that the probability of occurrence of an event is related to time or space by a coefficient **l**. The process is completely defined by this single parameter **l**, which is a measure for the average number of events per unit of distance (1D), space (2D) or time, as well as a measure for the variance of the distribution. The probability of the occurrence of i events over a distance, area or time interval x is given by:

$$P_i = \frac{\delta(\mathbf{l}x)^i}{i!}e^{K\mathbf{l}x} \qquad (8)$$

A typical feature of the Poisson distribution is the exponential frequency distribution of the interval x between two consecutive events. Two methods (1D, 2D) are presented to determine the single parameter **l** that characterizes the Poisson process, in order to verify whether the hypothesis of a Poisson process holds in space (2D) as well as after projection of clusters on a line (1D). The position of the clusters are determined by their center points (cfr. Eq. 7).

Number of clusters per unit length on an axis: 1D Poisson process

All center points of clusters are projected on four predefined axes. For this study two coordinate systems are defined: axes parallel to the image sides (North–South and East–West) and axes parallel with and perpendicular to the direction of the movement (Fig. 6a). If the projected positions (i.e. the coordinates on a projection axis) of the cluster centers are distributed by a Poisson process, then the distance between the projections should follow an exponential distribution. Through fitting (least squares method) an exponential distribution to the histogram of the distances between adjacent points, the parameter $\mathbf{l}_{1D}$, representing the number of clusters per unit of length, is retrieved.

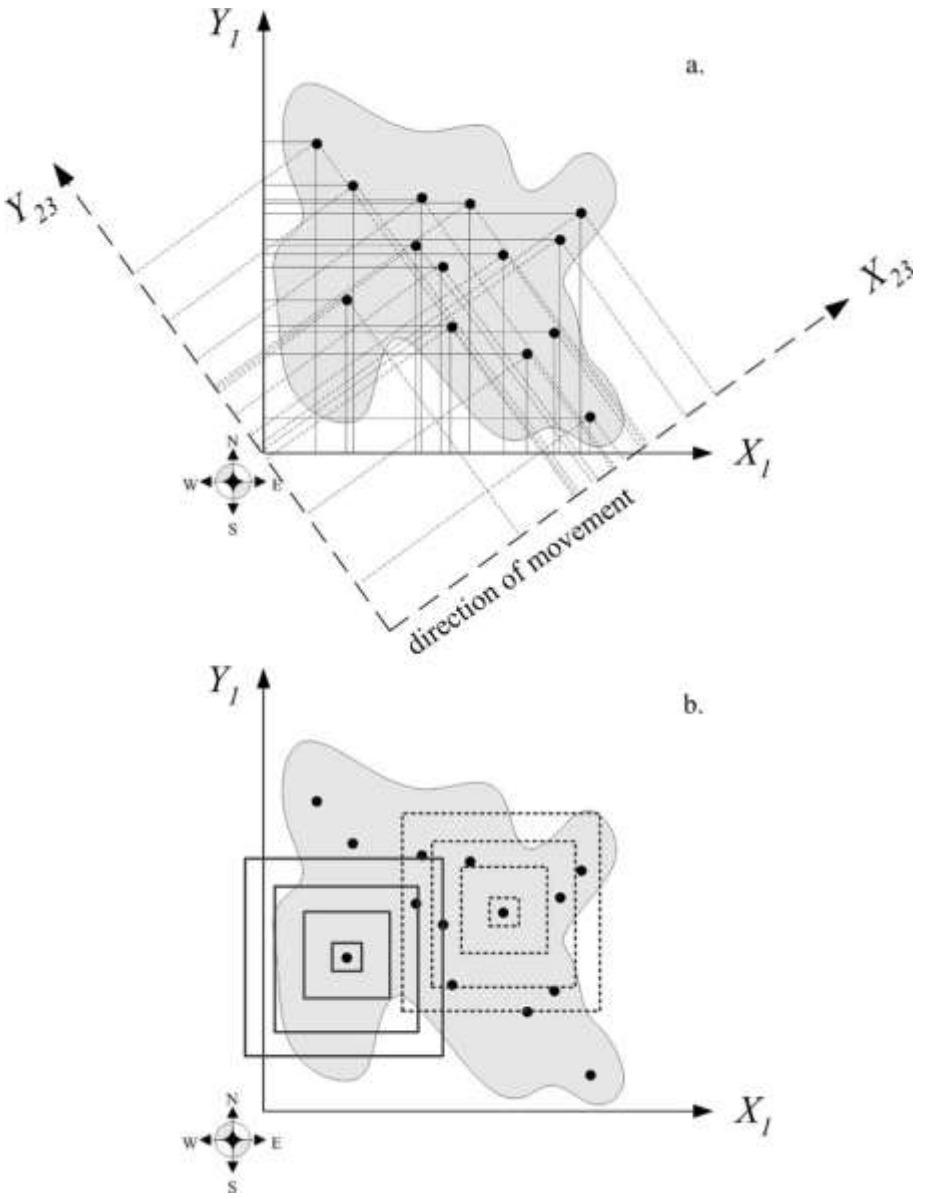

Fig. 6. Schematic overview of the methods to determine. (a) The number of clusters per unit of length after projection and (b) the number of clusters per unit area.

Number of clusters per area: 2D Poisson process

In a 2D Poisson process the λ_{2D} parameter represents the average number of clusters per unit of area. This means that with increasing area the number of clusters increases linearly, with a slope λ_{2D}. Starting with a square area surrounding a single cluster center, the square area centered around the first cluster center is gradually increased. For every new increased area the number of cluster centers is counted. This is repeated for each cluster center in the image. The number of clusters in a given area is calculated as the average number of clusters over all squares of the same size around each cluster (Fig. 6b). Finally, a line is

optimally fitted (least squares method) to the observed relation between the area and the number of clusters, and the parameter I_{2D} is retrieved from its slope.

7. Results and discussion

Descriptive statistics for all characteristics are calculated and statistical distributions are fitted to observed frequency distributions. These results give information that can be used directly into rainfall models. For the descriptive statistics simple sample averages, standard deviations, minima and maxima are studied. Furthermore non-parametric Mann–Whitney-*U* tests (Zar, 1999; McCuen, 2003) are performed to analyze differences between two variables. The null-hypothesis for these tests is that the distributions for both variables are the same. The higher the power to reject this hypothesis, the more likely the samples are really characterized by a different distribution.

The theoretical distribution functions are fitted based on a combination of non-parametric Kolmogorov-Smirnov tests (McCuen, 2003), *Q*–*Q* plots and curve fitting. The null-hypothesis for a Kolmogorov-Smirnov test is that the observed distribution of a sample is represented by a proposed theoretical distribution. The higher the power to reject this hypothesis, the less likely the theoretical distribution matches the observed one. In *Q*–*Q* plots the theoretical expected value of a random variable at a given probability is plotted against the observed value. The criterion for a good match between observed and theoretical distribution is an evaluation of the goodness-of-fit of this plot with the 1–1 line. A final tool used is curve fitting, where the best fit between an observed distribution and a theoretical distribution is found by a combination of visual interpretation and minimizing the least square error, while tuning the parameters defining the theoretical distribution. In this study normal, log–normal, gamma, exponential, Weibull and uniform distributions are compared for each characteristic variable. In an attempt to improve fits of theoretical distributions with observed distributions, also different transformations on each variable (V) are considered, e.g. $\log(V)$, $1/V$ and $\sqrt{V}$.

Velocity and direction of movement

Out of the 20 series of radar images, 1603 pairs of consecutive images are selected. For each of these pairs the movement was tracked by (i) following the mass center of the rainy areas over the whole image, (ii) following the mass centers of the isolated rainstorms and (iii) using the correlation method. Tracking the mass center of the total rainy area in a radar image reveals some serious drawbacks of the method. For example small rainy areas (sometimes with very high intensities) around the main rainstorm are not stable in time, i.e. they have a quite short lifetime (cfr. raincells). This affects the spatial distribution of rainfall and consequently the position of the mass center. Tracking the mass center of isolated rainstorms gives better results, but for a continuous analysis over a time series, there is the problem of rainstorms moving in or out of the image window, producing temporary unrealistic results for the direction and velocity of rainstorms.

The correlation method on the other hand, gives far more realistic results and is used for further analysis. As discussed in Section 3, increments for the spatial lags can be chosen as small as desired. In this study the increments are chosen at a tenth of the pixel size allowing to estimate the velocity at an accuracy of 0.24 km/15 min. Fig. 7 shows an example of the fact that due to the resampling, using weighted averages of fractions of pixels, local maxima are found in the behavior of the correlation coefficient. In the studied series, the optimal displacement vector is typically found when an image is displaced over a non-integer multiple of pixels or in other words, after smoothing the first image. It is interesting to note that Bellon and Zawadski (1994) found that radar based forecasts could be optimized, if pixel values first were averaged over a certain area, i.e. after smoothing. The loss of information by averaging (smoothing) can be well accepted, because most intense echoes only last a short time. Analogously, it can be expected that the correlation coefficient will increase for smoothed images, as the most intensive echoes will not occur at the same positions within a rainstorm in consecutive images.

Descriptive statistics for the analysis of all 20 series together are summarized in Table 2. Histograms of the data are made for the angle and velocity of the movement for every single radar image series and for

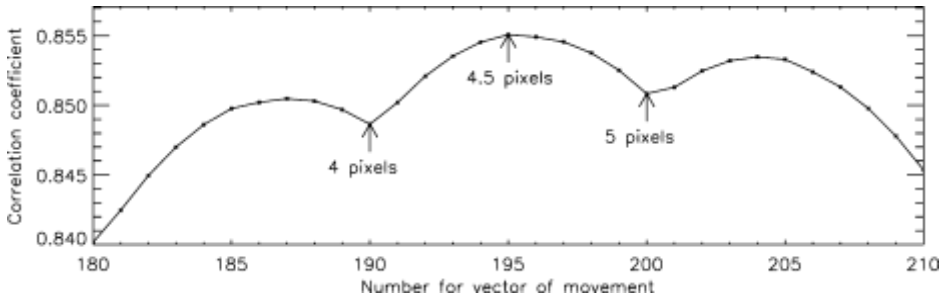

Fig. 7. Determination of the movement of the rainfall event of March 6, 1998 from 8:00 to 8:15 a.m. Detailed view of the correlation function around the maximum with indication of the number of pixels over which the image at 8:15 a.m. is horizontally shifted (under a constant angle of 0.1 rad). The optimal vector of movement is at 0.1 rad and a distance lag in the direction of movement of 10.85 km (rZ0.8551; RMSEZ 0.3715; vector number 195).

all analyzed images together. As expected, the histograms for single series show a rather narrow shape around the mean, while for all 20 series together the variance increases a lot. The normal distribution best matches the observed distribution for the angle of movement, while the Weibull distribution best fits to the observed distribution of the velocity. No transformation of the data improved the fit with any theoretical distribution for any of the two variables. The density functions of the normal distribution, $N(\mu,\sigma)$, and the two-parameter Weibull distribution, $W(a,b)$ are, respectively, given by:

$$f_x(x;\mu;\sigma^2) = \frac{1}{\sigma\sqrt{2\pi}} \exp\left[-\frac{(x-\mu)^2}{2\sigma^2}\right] \quad (9)$$

and

$$f_x(x;a;b) = \frac{b x^{b-1}}{a} \exp\left[-\left(\frac{x}{a}\right)^b\right] \quad (10)$$

The Weibull distribution for the velocity is characterized by a scale parameter a of 0.98 and a shape parameter b of 2.10 (Fig. 8). The velocity of the studied rainfall events varies between 0.03 and 3.09 km min^{-1}, with an average value of 0.86 km min^{-1} (Table 2). The normal distribution for the direction of the movement is characterized by a mean μ of 0.33 rad and a standard deviation σ of 0.75 rad (Fig. 8). The direction in which the rainfall event is moving varies between −2.88 and 2.90 rad relative to the eastern direction (Table 2). The studied rainfall systems mainly move in the East-North East direction, which is a consequence of typical weather

Table 2
Sample average *m*, standard deviation *s*, minimum min, maximum max and fitted distribution for the velocity and direction of movement (calculated on 1603 pairs of radar images) and for geometric characteristics (of 934 rainstorms): area, perimeter and dimensions, calculated using the three different methods

	m	*s*	min	max	Distribution
Velocity u_{xy} (km min^{-1})	0.863	0.412	0.030	3.088	W (aZ0.98, bZ2.10)
Direction angle φ (rad)	0.327	0.754	−2.880	2.900	N (μZ0.33, σZ0.75)
Area (km^2)	87178	35707	8456	202568	N ($\mu^{0.5}$Z288.90, $\sigma^{0.5}$Z60.96)
Perimeter (km)	3654	1174	1022	6989	N ($\mu^{0.5}$Z59.63, $\sigma^{0.5}$Z9.90)
s_{x1} (km)	382	90	79	480	–
s_{y1} (km)	405	75	94	480	–
s_{x2} (km)	328	117	81	609	W (aZ367.47, bZ3.06)
s_{y2} (km)	314	111	53	563	W (aZ351.66, bZ2.99)
s_{x3} (km)	410	104	124	618	W (aZ450.01, bZ4.43)
s_{y3} (km)	392	89	126	599	W (aZ425.71, bZ5.12)

A square root transformation of the data is indicated with a $^{0.5}$-subscript for the distribution parameters. The distributions are indicated as *N* and *W* for, respectively, the normal and Weibull distribution.

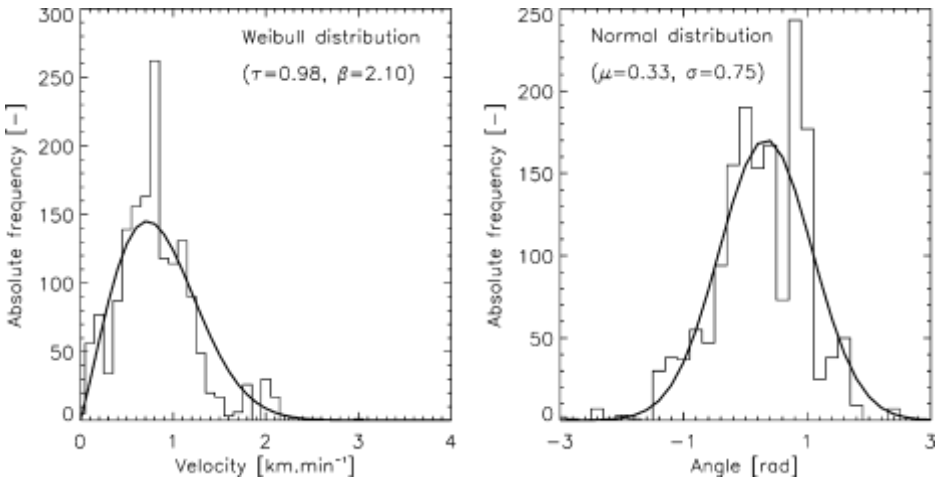

Fig. 8. Distributions for the velocity and direction (angle) of movement based on results for 1603 pairs of radar images.

conditions over the area in consideration (cfr. Section 2).

Using rain gauge measurements taken during 1994–1997 over Antwerp (Belgium), a region that is included in our radar images, Willems (1999) found an average velocity for raincells of 0.6 km min^{K1} and a direction of K0.38 rad. Probability distribution functions for the velocity of raincells and their direction of movement were also determined by Willems (1999, 2001). They found for raincells the same type of distributions as a best fit for observed histograms, with slightly different parameters. For the velocity (km min^{K1}) W(aZ0.70, bZ2.36) was found to match best with the observed distribution, while *N*(mZK0.38, sZ1.19) fitted best the observed distribution for the direction (rad). This indicates an agreement between the movement of cells and that of rainstorms in frontal systems over Belgium. For one limited series Zawadski (1973) found velocities around 1.1 km min^{K1} for cells and rainstorms in convective rain events observed with the McGill FPS-16 radar (Quebec, Canada). He found that the agreement between cell and storm speeds was very good during development and peak periods of the storm. Tsanis et al. (2002) reported an average rainstorm velocity of G1.0 km min^{K1} as a result of calculations using a radar storm tracker (applying cross-correlation technique) as well as a result obtained using a rain gauge technique (smaller scale) for rainfall events during one year in Canada.

Váldes et al. (1985) assumed in their rainfall model that cells and rainstorms move at the same speed and under an angle of 0 rad with velocities between 0.07 and 0.17 km min^{K1}, depending on the synthetic climate simulated. Mellor and O'Connell (1996) and Mellor and Metcalfe (1996) proposed methods to characterize raincells and rainstorms and applied them on synthetic data. Mellor and O'Connell (1996) estimated the velocity of real raincells over a catchment near Manchester (UK) around 0.95 km min^{K1} and Mellor and Metcalfe (1996) concluded from literature review that the velocity of storms range between 0.33 and 1.5 km min ^{K1}. Similar results are reported by, e.g. Niemczynowicz (1987), Kawamura et al. (1997) and Upton (2002).

Geometric characterization of rainstorms

The total area (km^2) and the perimeter (km) for isolated rainstorms are calculated. The results of this analysis are summarized in Table 2 and Fig. 9. Based on the analysis of 934 rainstorms, we found that the area of the rainstorm lies in the range 10^3–10^4 km^2, which means that we study synoptic areas and LMSAs (Austin and Houze, 1972). Statistical analyses revealed that the distribution of the area and the perimeter can be approached by a normal distribution after a square root transformation of the data. The mean m and standard deviation s are given by 288.90 and 60.96 km, respectively, for the square root

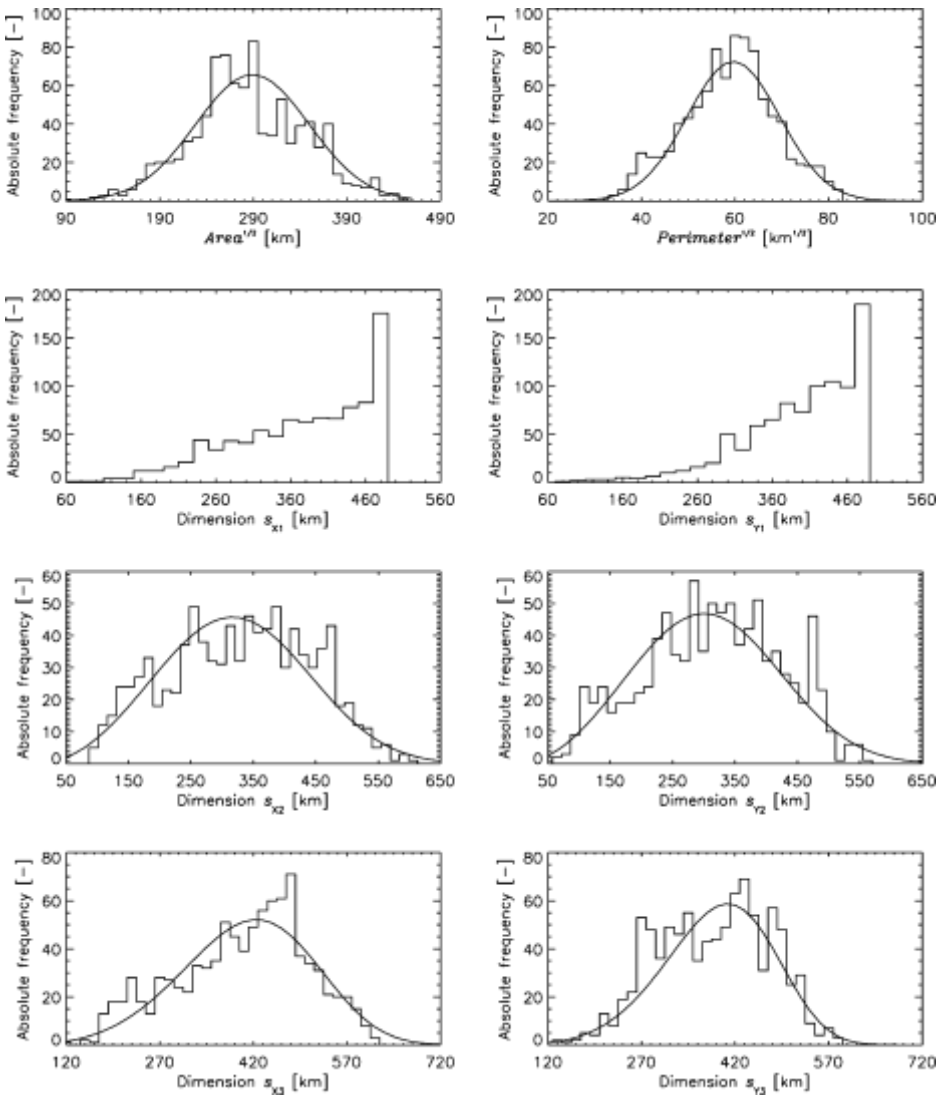

Fig. 9. Observed histograms and fitted distributions for different geometrical characteristics (area, perimeter, dimensions s_{x1}, s_{y1}, s_{x2}, s_{y2}, s_{x3} and s_{y3} obtained by method 1, 2 and 3) based on results for 934 rainstorms.

transformed area and 59.63 and 9.90 $km^{0.5}$ for the square root transformed perimeter.

The dimensions of rainstorms are analyzed by the three proposed methods. Descriptive statistics are summarized in Table 2 and Fig. 9 for the total of 934 rainstorms analyzed. The extent of the studied rainstorms is in average between 300 and 400 km. It is obvious that the size of the radar images can limit the analysis as the maximum dimension of rainstorms along the X_1 and Y_1 axis is limited to 480 km, the total width of the radar image and a maximum of 679 m for the $X_{2,3}$ and $Y_{2,3}$ axes. For method 3, a cutoff of the histograms for higher values is not seen, while for method 1, there is a clear cutoff. Consequently, the distributions for the s_{x1} and s_{y1} variables are not calculated. Method 3 results in larger dimensions for the rainstorms compared with the dimensions calculated with method 2. For the variables s_{x2}, s_{x3}, s_{y2}

and s_{y3} a Weibull distribution fits best with the observed distributions, with shape parameters of, respectively, 3.06, 4.43, 2.99 and 5.12 and scale parameters of, respectively, 367.47, 450.01, 351.66 and 425.71. No transformation of any of the variables improved the fit.

A Mann–Whitney-*U* test on the s_{x2}, s_{y2} and the s_{x3}, s_{y3} data showed a significant difference between the dimensions of the rainstorm in the direction of the rainfall movement and the direction perpendicular to the direction of movement (P ! 0.05), for both methods 2 and 3. The extent of a rainstorm in the direction of the movement is in general slightly larger than the extent perpendicular to the direction of the movement (see Fig. 9). From the analysis of the individual storms, it was found that for the smaller rainstorms, dimensions in the two directions differ more from each other than for larger rainstorms, which seem to have a less elongated shape. Image windows of larger size should be considered in order to generalize this result, as due to the limited image window some rainstorms are not completely visualized (see distributions of s_{x1} and s_{y1} in Fig. 9).

Because the dimensions of the rainstorms will be used to define a rainstorm in a spatial rainfall model, the observed rainstorm area is compared with the area of an ellipse. This allows to account for the statistically significant dimensions of the geometrical shape in two perpendicular directions. Based on the deviations from the 1–1 line in Fig. 10 it is clear that dimensions obtained by method 1 and method 3 tend to give an overestimation of the rainstorm area, while dimensions obtained by method 2 give a quite good approximation of the total area of rainstorms.

Distribution of clusters in space

In order to describe the distribution of clusters in a rainstorm area, a 1D and a 2D Poisson process can be used. For the characterization of the 1D Poisson distribution, histograms of distances between adjacent projected clusters are constructed and exponential distributions are fitted by tuning the λ_{1D} parameter. This analysis is performed for four directions: East–West and North–South direction and the direction parallel with and perpendicular to the direction of the rainstorm movement. The histograms closely fit the exponential distributions, which supports the assumption that the *x*- and *y*-coordinates of clusters follow a Poisson process. For every series separately and for the 20 series together exponential distributions are fitted for the four directions individually (Fig. 11). In East–West direction an average of 0.199 clusters km^{K1} is found, while in North–South direction 0.211 clusters km^{K1} are counted. In the direction of the movement 0.135 clusters km^{K1} ($\lambda_{1D,s}$) are found and perpendicular to the direction of the movement an average $\lambda_{1D,\perp}$ of 0.145 clusters km^{K1} is retrieved. In general there is a slightly larger distance between projections of cluster centers in the direction of the movement. This could be partially caused by the slightly elongated shape of rainstorms in the direction of the movement.

The characterization of the 2D Poisson process is performed by plotting the average number of clusters

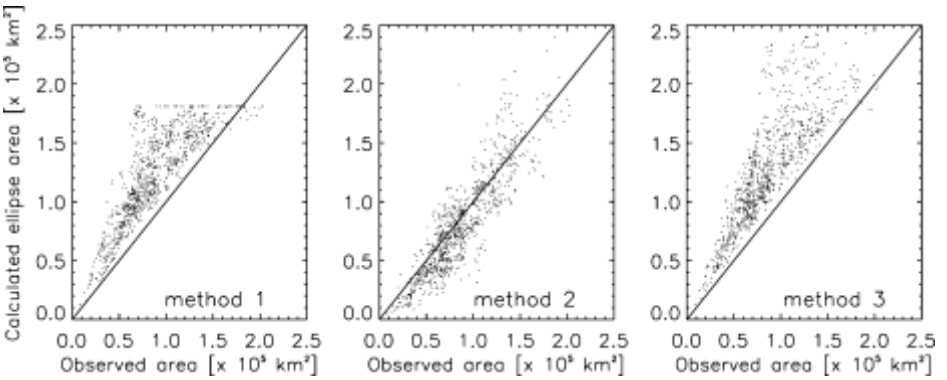

Fig. 10. Comparison of the observed rainstorm area with the area of an ellipse calculated based on the dimensions resulting from method 1 (RMSEZ0.413X10^5 km^2), method 2 (RMSEZ0.202X10^5 km^2) and method 3 (RMSEZ0.481X10^5 km^2).

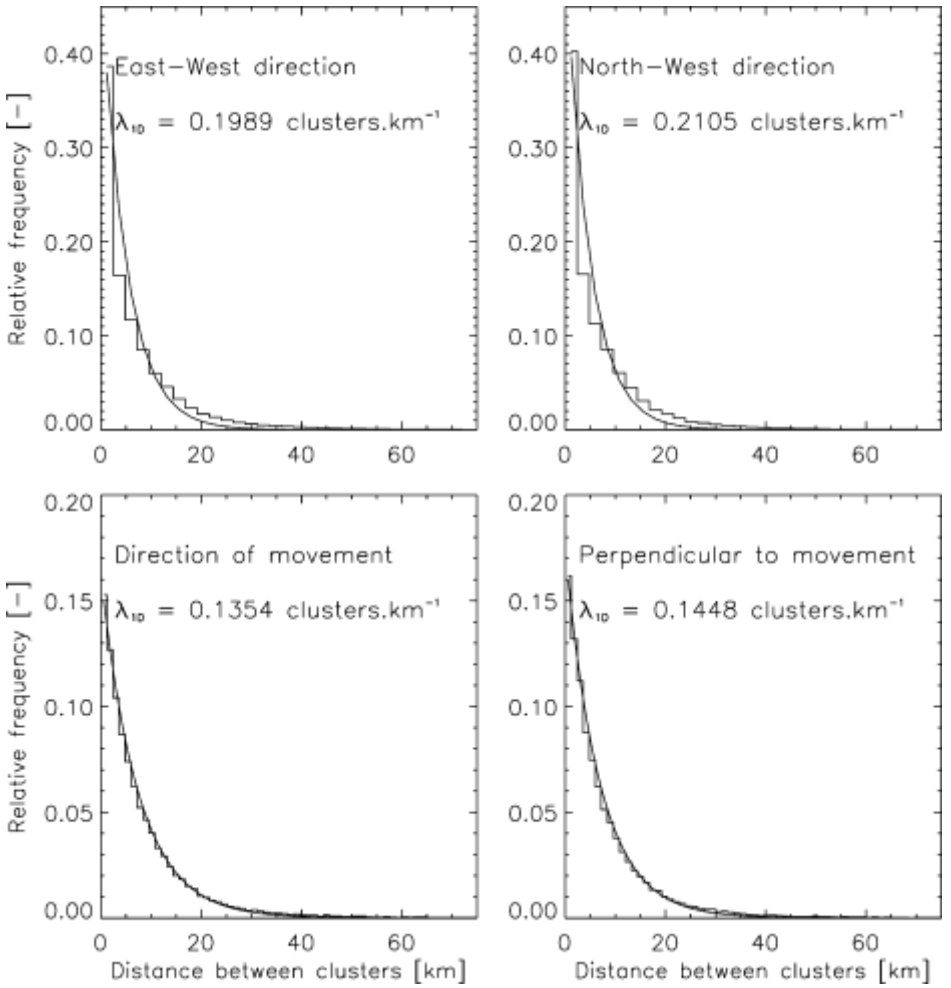

Fig. 11. Exponential distribution of the distance between clusters after projection on axes in four different directions to determine I_{1D} for all 20 series. The histograms are cut off at a distance of 75 km between clusters.

(and the standard deviation on it) for increasing areas of rainfall and fitting a straight line (Fig. 12). Again this is done for all individual image series and for all images together. Only the first linear part of the plot should be taken into consideration. Large rainy areas are not available in all images and so for larger areas less images are available to contribute to the average number of clusters in those areas. From all 20 series together, the parameter I_{2D} is quantified as (5.56G 1.91)X10^{K4} clusters km^{K2}. Bacchi et al. (1996) reported a cluster density of 4.11X10^{K4} clusters km^{K2} as a parameter in a Neyman-Scott based model. This result was found on radar images with a resolution of 2X2 km^2. They found slightly higher values on radar images with a higher resolution.

The clusters only occur within the limited area of a rainstorm and consequently the related Poisson processes are restricted to this rainstorm area. A changing rainstorm size does not influence the I_{2D} value, assuming a homogeneous Poisson process in space. However, as the bounded rainstorm area limits the number of clusters projected on the axes, the value for I_{1D} is dependent on the rainstorm area. A combination of the results from the 1D and 2D method provide information on the extent of the rainstorm. Let us assume that a rainstorm can be

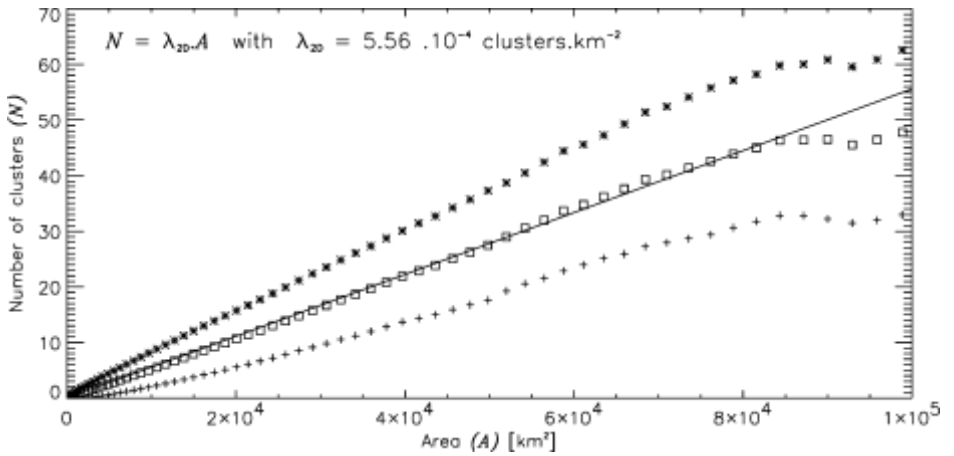

Fig. 12. Average (➢) number of clusters plus and minus the standard deviation (resp. * and C) for increasing areas, to determine λ_{2D} for all 20 series.

represented by an ellipse with major diameter s_x (along the direction of the movement) and minor diameter s_y (perpendicular to the direction of movement). The number of clusters within a rainstorm can then be written as

$$\lambda_{2D} \frac{p}{4} s_x s_y \lambda_{1D,s} s_x \quad (11)$$

and

$$\lambda_{2D} \frac{p}{4} s_x s_y \lambda_{1D,T} s_y \quad (12)$$

where $\lambda_{1D,s}$ and $\lambda_{1D,T}$ are the parameters of the 1D Poisson distribution, respectively, along and perpendicular to the direction of movement and λ_{2D} is the parameter of the Poisson distribution in 2D. From Eqs. (11) and (12) the dimensions in both directions can be estimated by

$$s_x \frac{4}{p} \frac{\lambda_{1D,T}}{\lambda_{2D}} \approx 332 \text{ km} \quad (13)$$

$$s_y \frac{4}{p} \frac{\lambda_{1D,s}}{\lambda_{2D}} \approx 309 \text{ km} \quad (14)$$

which corresponds to the values s_{x2} (Z328 km) and s_{y2}(Z314 km) given in Table 2.

8. Conclusions

Several characteristics of rainfall events occurring in frontal weather systems over a temperate area, are investigated and statistical descriptors and distributions are proposed for use in rainfall models. The movement of rainstorms is described by its direction and velocity. The correlation technique is the most successful to determine these variables. Statistical analysis reveals that the velocity of rainfall events follows a two-parameter Weibull distribution and that the direction of rainfall movement follows a normal distribution. The studied rainfall events move at an average velocity of 0.86 km min^{K1} under a direction of 0.327 rad relative to the eastern direction.

A technique to discriminate single rainstorms within radar images is developed, using the temporal evolution of the total area and the total perimeter of all rainy areas in the radar image. Only images with a fully developed rainstorm are selected for further analysis. Three methods to determine rainstorm dimensions are proposed. Comparison of the real rainstorm area with the area calculated from the rainstorm dimensions supports the use of the dimensions resulting from the method 2. In this method the origin of the coordinate system is situated in the rainstorm center and the directions are based on

the direction of movement. The rainstorm is characterized by the dimensions of a rectangle whose sides are determined by the intersection of the coordinate axes with the rainstorm boundaries. The distributions of the dimensions in the direction of the movement and perpendicular to it, are both described by a two-parameter Weibull distribution. Furthermore, the dimensions of the rainstorms are significantly different for both directions.

The spatial distribution of clusters in rainstorms is evaluated by two methods in which the parameter **l** that describes a Poisson process is calculated. In a first method the number of clusters per unit length is determined after projection of the cluster centers. A value of 0.135 and 0.145 clusters km^{K1} is found in the direction along and perpendicular to the movement of the rainstorm, respectively. In a second method the number of clusters per unit of area is calculated after counting the number of clusters in increasing areas within rainstorms. This method results in a value of $(5.56G1.91)X10^{K4}$ clusters km^{K2}. By a combination of the results from both methods, an estimate of the rainstorm extent can be obtained.

Analysis of more rainfall events, covering different types of rainfall would be a useful extent of this research in order to capture a broad range of rainfall types in statistical descriptions. Also the use of different types of radar images, more specifically with different resolutions, could be advised to pick up even more variation and to investigate possible scaling effects. Implementation of accurate descriptions of rainfall patterns in rainfall models is desirable to assure realistic representations of the natural rainfall process. This will definitely increase the accuracy of rainfall inputs in hydrological models and improve their results.

References

Amorocho, J., Wu, B., 1977. Mathematical models for the simulation of cyclonic sequences and precipitation fields. J. Hydrol. 32, 329–345.

Arnaud, P., Bouvier, C., Cisneros, L., Dominguez, R., 1999. Influence of rainfall spatial variability on flood prediction. J. Hydrol. 260, 216–230.

Austin, P., 1960. Microstructure of storms as described by quantitative radar data, in: Weichman, H. (Ed.), Physics of Precipitation. Waverly Press, Baltimore, pp. 86–93.

Austin, P., Houze, R., 1972. Analysis of the structure of precipitation patterns in New England. J. Appl. Meteorol. 11, 926–935.

Bacchi, B., Ranzi, R., Borga, M., 1996. Statistical characterization of spatial patterns of rainfall cells in extratropical cyclones. J. Geophys. Res. 101, 277–286.

Bellon, A., Zawadski, I., 1994. Forecasting of hourly accumulations of precipitation by optimal extrapolation of radar maps. J. Hydrol. 157, 211–233.

Bergeron, T., 1960. Problems and methods of rainfall investigation, in: Weichman, H. (Ed.), Physics of Precipitation. Waverly Press, Baltimore, pp. 5–30.

Berndtsson, R., Niemczynowicz, J., 1986. Spatial and temporal characteristics of high-intensive rainfall in northern Tunisia. J. Hydrol. 87, 285–298.

Berndtsson, R., Jinno, K., Kawamura, A., Larson, M., Niemczynowicz, J., 1994. Some Eulerian and Lagrangian statistical properties of rainfall at small space–time scales. J. Hydrol. 153, 339–355.

Blackmer, R., Duda, R., 1972. Application of pattern recognition techniques to digitised radar data. In: 15th Radar Meteorological Conference. Champaign-Urbana, pp. 138–143.

Bonser, J., Wong, A., 1987. A feature based method for tracking mesoscale rainfall areas in radar images. Stochastic Hydrol. Hydraul. 1, 185–198.

Bras, R., Rodr´ıguez-Iturbe, I., 1976. Rainfall generation: a nonstationary timevarying multidimensional model. Water Resour. Res. 12, 450–456.

Brémaud, P., Pointin, Y., 1993. Forecasting heavy rainfall from rain cell motion using radar data. J. Hydrol. 142, 373–389.

Bruce, J., Clark, R., 1966. Introduction to Hydrometeorology. Pergamon Press, Oxford.

Burlando, P., Montanari, A., Ranzi, R., 1996. Forecasting of storm rainfall by combined use of radar, rain gages and linear models. Atmos. Res. 42, 199–216.

Chaubey, I., Haan, C., Grunwald, S., Salisbury, J., 1999. Uncertainty in the model parameters due to spatial variability of rainfall. J. Hydrol. 220, 48–61.

Chen, Z., Kavvas, M., 1992. An automated method for representing, tracking and forecasting rain fields of severe storms by Doppler weather radars. J. Hydrol. 132, 179–200.

Collier, C., 1989. Applications of Weather Radar Systems. A Guide to Uses of Radar Data in Meteorology and Hydrology. Ellis Horwood, Chichester.

Cowpertwait, P., 1995. A generalized spatial-temporal model of rainfall based on a clustered point process. Proc. R. Soc. Lond. A 450, 163–175.

Cowpertwait, P., Kilsby, C., O'Connell, P., 2002. A space–time Neyman–Scott model of rainfall: Empirical analysis of extremes. Water Resour. Res. 38, 61–614.

Cox, D., Isham, V., 1980. Point Processes. Chapman & Hall, London.

De Troch, F., Heynderickx, J., Troch, P., Van Erdeghem, D., 1990. On the usefulness of weather radar data in real time hydrological forecasting in belgium, in: Collier, C., Chapuis, M. (Eds.), Weather Radar Networking. Seminar on COST Project 73. Kluwer, Dordrecht, pp. 462–470.

Eagleson, P., 1972. Dynamics of flood frequency. Water Resour. Res. 8, 878–898.

Eagleson, P., 1984. The distribution of catchment coverage by stationary rainstorms. Water Resour. Res. 20, 581–590.

Gelfand, I., Vilenkin, N., 1964. Generalised Functions, vol. 4. Academic Press, Orlando.

Gupta, V., Waymire, E., 1979. A stochastic kinematic study of subsynoptic space–time rainfall. Water Resour. Res. 15, 637–644.

Gupta, V., Waymire, E., 1987. On Taylor's hypothesis and dissipation in rainfall. J. Geophys. Res. 92, 9657–9660.

Heylen, R., Maenhout, A., 1994. Introduction to Radar Meteorology (in Dutch). Koninklijk Meteorologisch Instituut van Belgie¨ (KMI).

Hobbs, P., Locatelli, J., 1978. Rainbands, precipitation cores and generating cells in a cyclonic storm. J. Atmos. Sci. 35, 230–241.

Jinno, K., Kawamura, A., Berndtsson, R., Larson, M., Niemczynowicz, J., 1993. Real-time rainfall prediction at small space–time scales using a two-dimensional stochastic advection–diffusion model. Water Resour. Res. 29, 1489–1504.

Kavvas, M., Puri, P., 1983. A stochastic model of the extratropical cyclonic precipitation field formed around a low pressure center. EOS Trans. 64, 221.

Kawamura, A., Jinno, K., Berndtsson, R., Furukawa, T., 1997. Real-time tracking of convective rainfall properties using a two-dimensional advection–diffusion model. J. Hydrol. 203, 109–118.

KMI, 1998–2000. Monthly Bulletins. Climatological Observations (Part I). Koninklijk Meteoreologisch Instituut van Belgie (KMI), Ringlaan 3, B-1180 Brussels, Belgium 1998–2000 (in Dutch).

Krajewski, W., Lakshmi, V., Georgakakos, K., Jain, S., 1991. A Monte Carlo study of rainfall sampling effect on a distributed catchment model. Water Resour. Res. 27, 119–128.

Krajewski, W., Raghavan, R., Chandrasekar, V., 1993. Physically based simulation of radar rainfall data using a space-time rainfall model. J. Appl. Meteorol. 32, 268–283.

Kumar, P., Foufoula-Georgiou, E., 1993. A multicomponent decomposition of spatial rainfall fields 2. Self-similarity in fluctuations. Water Resour. Res. 29, 2533–2544.

Le Cam, L., 1961. A stochastic description of precipitation, In: Proceedings Fourth Berkeley Symposium on Mathematics, Statistics, and Probability, vol. 3. University of California Press, pp. 165–186.

Mason, B., 1970. Future developments in meteorology: an outlook to year 2000. Q. J. R. Meteorol. Soc. 96, 349–368.

McCuen, R.H., 2003. Modeling Hydrologic Change—Statistical Methods. Lewis, Boca Raton.

Mellor, D., 1996. The Modified Turning Bands (MTB) model for space-time rainfall. I. Model definition and properties. J. Hydrol. 175, 113–127.

Mellor, D., Metcalfe, A., 1996. The Modified Turning Bands (MTB) model for space–time rainfall. III. Estimation of the storm/rainband profile and a discussion of future model prospects. J. Hydrol. 175, 161–180.

Mellor, D., O'Connell, P., 1996. The Modified Turning Bands (MTB) model for space–time rainfall. II. Estimation of raincell parameters. J. Hydrol. 175, 129–159.

Niemczynowicz, J., 1987. Storm tracking using rain gauge data. J. Hydrol. 93, 135–152.

Niemczynowicz, J., Jönsson, O., 1981. Extreme rainfall events in Lund 1979–80. Nord. Hydrol. 12, 129–142.

Obeysekera, J., Tabios III., G., Salas, J., 1987. On the parameter estimation of temporal rainfall models. Water Resour. Res. 23, 1837–1850.

Obled, C., Wendling, J., Beven, K., 1994. The sensitivity of hydrological models to spatial rainfall patterns: an evaluation using observed data. J. Hydrol. 159, 325–333.

Peters-Lidard, C., Wood, E., 1994. Estimating storm areal average rainfall intensity in field experiments. Water Resour. Res. 30, 2119–2131.

Rodr´ıguez-Iturbe, I., 1986. Scale of fluctuation of rainfall models. Water Resour. Res. 22, 15S–37S.

Rodr´ıguez-Iturbe, I., Eagleson, P., 1987. Mathematical models of rainstorm events in space and time. Water Resour. Res. 23, 181–190.

Shah, S., O'Connel, P., Hosking, J., 1996. Modelling the effects of spatial variability in rainfall on catchment response. 1. Formulation and calibration of a stochastic rainfall field model. J. Hydrol. 175, 67–88.

Shih, S., 1982. Rainfall variation analysis and optimization of gaging systems. Water Resour. Res. 18, 1269–1277.

Taylor, G., 1938. The spectrum of turbulence. Proc. R. Soc. Lond. A 164, 1–476.

Tsanis, I., Gad, M., Donaldson, N., 2002. A comparative analysis of rain-gauge and radar techniques for storm kinematics. Adv. Water Res. 25, 305–316.

Upton, G., 2002. A correlation–regression method for tracking rainstorms using rain-gauge data. J. Hydrol. 261, 60–73.

Váldes, J., Rodriguez-Iturbe, I., Gupta, V., 1985. Approximations of temporal rainfall from a multidimensional model. Water Resour. Res. 21, 1258–1270.

Waymire, E., 1984. A spectral theory of rainfall intensity at the meso-b scale. Water Resour. Res. 20, 1453–1465.

Waymire, E., Gupta, V., 1981a. The mathematical structure of rainfall representations 1. A review of the stochastic rainfall models. Water Resour. Res. 17, 1261–1272.

Waymire, E., Gupta, V., 1981b. The mathematical structure of rainfall representations 2. A review of the theory of point processes. Water Resour. Res. 17, 1273–1285.